PAPER

A mechanically tough and ultra-swellable microneedle for acute gout arthritis†

Suping Jiang,‡[a] Wen Wang,‡[a] Jiming Ke,‡[a] Shan Huang,[a] Jie Wang,[a] Chengxi Luo,[a] Xiaoxia Li,[a] Kaili Zhang,[a] Huanhuan Liu,*[a,b,c,d] Wensheng Zheng,*[a,e] Jiwen Zhang*[a,f] and Can Peng*[a,b,g,h]

Acute gout arthritis (AGA) remains the fundamental research focus in the entire medical field. Hydrogel microneedles (HMNs) loaded with therapeutic molecules such as colchicine (Col) have been developed as a new tool for the management of AGA in a minimally invasive manner. However, the incompatible mechanical and swelling properties of HMNs limited the diffusion of the drug from the HMN system, which remains a challenge for practical use. Here, a mechanically tough (11.53 N per needle) and super-swelling (2708%) hydrogel microneedle (HMNs) composed of a uniform network structure was developed using a UV-responsive crosslinker through *in situ* photopolymerization for percutaneous delivery of Col. Such HMNs and Col loaded HMNs (Col-HMNs) present excellent biocompatibility. Moreover, Col-HMNs present considerable anti-inflammatory effects *in vivo* through down-regulated inflammatory responses such as related cytokines IL-1β, IL-6, and TNF-α. These results demonstrated that the mechanically tough and super-swelling HMNs could be a promising tool for effective Col delivery to relieve AGA.

Introduction

Gout triggered by the accumulation of monosodium urate (MSU) crystals is a common form of inflammatory arthritis in both developed and developing countries.[1] Acute gout arthritis (AGA) causes stiffness in the affected joints as well as severe pain, affecting daily life seriously.[2] Thus, AGA has been one of the fundamental research focuses in the medical field.[3,4] At present, several effective treatments are used to relieve the pain and inflammation response in AGA by reducing the inflammatory response by suppressing multiple inflammatory factors such as tumor necrosis factor (TNF)-α, interleukin (IL)-6, and IL-1β levels and inhibiting inflammatory cell function, and they involve non-steroidal anti-inflammatory drugs (NSAID), corticosteroids and colchicine.[5–7] However, the above drugs are used orally or injected and are accompanied by serious side effects, failing AGA treatment.[8–10]

Microneedles (MNs) as a novel and promising medical tool, have been developed for painless transdermal drug delivery and relatively safe use for patients.[10–15] Hydrogel microneedles (HMNs), with excellent biocompatibility and phase transition properties, have widespread applications in the medical field.[13,16,17] However, the heterogeneous distribution of crosslinking points in the traditional hydrogels in a polymer network mostly produced weak and brittle HMNs, leading to limited application in the thick cuticle skin such as in elbow joints.[18–22] Furthermore, HMNs swell by imbibing the interstitial skin fluid and facilitate drug transport from the reservoir attached at the base into the skin.[23] Thus, the swelling capacity of HMNs plays a significant role in the drug release procedure. The application of microneedles with both tough mechanical and excellent swelling capabilities is rarely reported. Therefore, developing hydrogel microneedles with high swelling and mechanically tough properties for AGA treatment is significantly anticipated.

Here, we present an effective and facile strategy to obtain HMNs by *in situ* polymerization using a UV-responsive crosslinker with an ultraviolet light-responsive disulfide bond. The

[a]School of Pharmacy, Anhui University of Chinese Medicine, Hefei, Anhui, 230012, China. E-mail: huanhuanliu2016@ahtcm.edu.cn
[b]Anhui Province Key Laboratory of Pharmaceutical Preparation Technology and Application, Heifei, Anhui, 230012, China
[c]Engineering Technology Research Center of Modernized Pharmaceutics, Anhui Education Department (AUCM), Hefei 230012, China
[d]Institute of Pharmaceutics, Anhui Academy of Chinese Medicine, Hefei 230012, China
[e]Institute of Materia Medica, Chinese Academy of Medical Sciences and Peking Union Medical College, Beijing, 100050, China
[f]Center for Drug Delivery System, Shanghai Institute of Materia Medica, Chinese Academy of Sciences, Shanghai 201203, China
[g]Anhui Province Key Laboratory of Chinese Medicinal Formula, Hefei, Anhui, 230012, China
[h]Institute of TCM Resources Protection and Development, Anhui Academy of Chinese Medicine, Hefei, Anhui, 230012, China. E-mail: pengcan@ahtcm.edu.cn

†Electronic supplementary information (ESI) available. See DOI: https://doi.org/10.1039/d2bm01937j

‡These authors contributed equally.

regular and well-defined network of the PAM hydrogel endows the microneedle with high mechanical toughness (11.53 N per needle) and super-swelling capability (2708%). Significantly, a controlled swelling procedure was used to load colchicine for enhanced efficiency and capacity. The cumulative release rate of colchicine reached as high as $(81.50 \pm 5.97)\%$ within 48 h. In addition, the remarkable biocompatibility of HMNs loaded with colchicine (Col-HMNs) had been demonstrated to play a positive role in relieving the inflammatory effects of MSU-induced acute gout by reducing the levels of inflammatory cytokines IL-1β, IL-6, and TNF-α, indicating its tremendous potential for AGA treatment.

Experimental section

Materials, animals, and cells

Colchicine was obtained from the China Institute of Food and Drug Inspection (99%, Beijing, China). Acrylamide was obtained from Saen (AR, 99.0%, Shanghai, China). N,N'-Bis (acrylyl)cysteamine was obtained from Alfa Aesar (98%, AlFA, UK). N,N-Methylenebisacrylamide was purchased from Macklin (99%, Shanghai, China). Irgacure 2959 was obtained from Sigma-Aldrich (98%, Shanghai, China). $K_2O_8S_2$ (99.5%) and calcein (98%) were obtained from Aladdin (Beijing, China). Carboxymethyl cellulose (CMC, AR) was obtained from Guangdong Wengjiang Chemical Reagent Co., Ltd (Guangdong, China). PDMS mold was obtained from Taizhou Microchip Medical Technology Co., Ltd (Taizhou, China). Colchicine tablets were obtained from Banna Pharmaceutical Co., Ltd (M.L. N.: H 53021369, Xishuangbanna, China). Penicillin, Streptomycin and FBS were obtained from Wolcavi (Beijing, China). DMEM complete medium was obtained from Sikejie (Shandong, China). CCK-8 was obtained from Skojiewei (Xi'an, China). The enzyme immunoassay (IL-1β, TNF-α, and IL-6) kit was obtained from Genomei (Wuhan, China). A Bradford protein assay kit was obtained from Beyotime (Shanghai, China). A myeloperoxidase assay kit was obtained from Jiancheng (Nanjing, China). Water mentioned in this work was Milli-Q distilled deionized water (18 MΩ cm^{-1}, Millipore Co.).

All animal procedures were performed in accordance with the Guidelines for Care and Use of Laboratory Animals of the Anhui University of Chinese Medicine and approved by the Animal Ethics Procedures and Guidelines of the People's Republic of China (animal ethics number: AHUCM-rats-2019001). Male Sprague-Dawley (SD) rats (weighing 250 ± 20 g) were obtained from the Anhui University of Chinese Medicine Laboratory Animal Resources Center. The rats were housed under standardized conditions of animal facilities with 6 rats in each cage (24 °C with 12 h of light/dark cycle). They were fed standard laboratory chow and water *ad libitum*.

Human immortalized keratinocytes (HaCaT) were purchased from Jiangsu KeyGEN BioTECH Corp., Ltd. The cells were separately cultured in DMEM containing 10% FBS and 1% penicillin–streptomycin in an incubator containing 5% CO_2 at 37 °C.

Instruments and characterization

An optical microscope, a fluorescence inverted microscope and a confocal laser scanning microscope were obtained from Leica Microsystems (Shanghai) Trading Co., Ltd (Shanghai, China). A scanning electron microscope was obtained from Thermo Fisher Scientific (China) Co., Ltd (Shanghai, China). A TMS-PILOT texture analyzer was obtained from Food Technology Corporation (USA). A DHC-6TD automatic transdermal instrument was obtained from Shanghai Logan Instrument Equipment Co., Ltd (Shanghai, China). A high-performance liquid chromatograph (HPLC) was obtained from Waters Corporation (USA). An FT-IR spectrometer was obtained from PerkinElmer, Inc. (Shanghai, China). A microplate reader was obtained from Molecular Devices Co., Ltd (i3x, Molecular Devices, USA). A toe volume measuring instrument was obtained from Beijing Zhongshidichuang Science and Technology Development Co., Ltd (Beijing, China). The IVIS Spectrum was obtained from PerkinElmer (USA).

Fabrication of HMNs

HMNs were fabricated using PDMS molds. The microneedle arrays consisted of 400 conical needles (20 × 20) with a height of 600 μm, a base width of 300 μm, and a tip spacing of 700 μm. Firstly, to prepare the pre-gel solution, the desired content of AM, BACA, and Irgacure 2959 was gradually dissolved in deionized water (DI) and further ultrasonicated for 5 min. Then, the pre-gel solution was poured into PDMS molds and centrifuged (3500 rpm, 5 min) to fill the tip with the liquid, and ultrasound was used to eliminate bubbles. Then, the mold filled with the pre-gel solution was exposed to UV light (365 nm, 300 W) for 20 min, thoroughly dried in an oven and demolded, and then HMNs were obtained. Colchicine solution (10 mg mL^{-1}, 100 μL) was added to the HMNs in the mold to swell for 12 h at −4 °C, dried in an oven and demolded, and then colchicine loaded HMNs (Col-HMNs) were obtained. In the same way, calcein was substituted for Col to prepare calcein-HMNs; furthermore, the control sample carboxymethyl cellulose (CMC) dissolving microneedles (CMC-DMNs) was also fabricated. 2.5% (w/v) CMC powder was added to water and stirred to swell initially. Then, the CMC gel (1 g) was poured into the microneedle mold, filled with the tip under vacuum for 10 min, fully dried, and carefully removed from the PDMS mold.

Mechanical strength evaluation

The mechanical strength of the microneedle was determined using the compression mode of the TMS-PILOT texture analyzer. A single needle was taken from the HMNs, fixed on the cover slide with a layer of condensed water vapor with the tip facing up and then placed on the stainless-steel platform of the texture analyzer. The cylindrical probe with a diameter of 6 mm was dropped at a speed of 30 mm min^{-1}, and the force was recorded continuously until a displacement of 40% of the microneedle height was reached.

In vitro skin insertion capability of HMNs

HMNs were manually inserted into fresh rat skin for 10 min and then removed. Then, 100 μL of 1% methylene blue solu-

tion was evenly distributed on the above skin for 10 min. After washing the residual methylene blue solution with normal saline and filter paper, the skin was observed using a digital camera.[24]

Calcein-HMNs were applied to porcine skin for 24 h. The skins were immediately cut into 5 μm thick sections with a freezing microtome and then observed using a confocal laser scanning microscope (CLSM).[25]

Measurement of the swelling ability

The swelling ability of the HMNs was calculated using the equation $(M_t - M_0)/M_0$, in which M_0 and M_t represent the weight of the HMNs before and after being immersed in PBS for 0–24 h.

In vitro transdermal release studies

The *in vitro* transdermal delivery of Col was studied using the DHC-6TD automatic transdermal instrument. Col-HMNs and Col-loaded CMC-DMN patches were firmly inserted into fresh rat skin which was already balanced in PBS for 30 min and fixed between the donor compartment and the receiver compartment. PBS (pH 7.4) was automatically filled in the receiver compartment at 37 °C, and magnetically stirred at 600 rpm. At predetermined time points, 1 mL of the sample from the receiver compartment was automatically taken out and refilled with 1 mL PBS simultaneously.

The COL concentrations of the samples were quantitatively analyzed by HPLC (Waters Corporation, USA) equipped with a Unitary C_{18} (4.6 mm × 250 mm, 5 μm) column. The mobile phase was methanol–water (55 : 45). The column temperature was 30 °C, the detection wavelength was 254 nm, the injection volume was 10 μL, and the flow rate was 1.0 ml min^{-1}. The colchicine concentration was calculated using a calibration curve ($y = 0.6294x - 0.0113$, $R^2 = 1$). Q_n (cumulative release) was calculated using formula (1) and fitted according to the first-order equation (formula (2)).

$$Q_n = VC_n + \sum_{i=1}^{n-1} C_i V_i \tag{1}$$

$$\log(1 - M_t/M_\infty) = -kt \tag{2}$$

The *in vitro* skin penetration behavior of drugs was investigated using fluorescent calcein loaded HMNs. At predetermined time points, the Bama miniature pig skin was cleaned and cut into 5 μm thick sections with a freezing microtome, and then observed under a confocal laser scanning microscope (CLSM).

Loading efficiency

Firstly, Col-loaded CMC-DMNs (1 mg Col) and Col-loaded HMNs (1 mg Col) were placed in 5 mL of PBS solution (pH 7.4) separately for 48 h to ensure that the microneedles were completely dissolved or at the swelling equilibrium. To precipitate the polymer, each sample solution (2 mL) was centrifuged at 5000 rpm for 10 min using an Amicon® Ultra filter (MW cut-offs < 100 kDa). The filtrate was then analyzed using HPLC. Finally, the percentage of loading efficiency was calculated using the equation (actual amount of drug (mg))/(initial amount of drug (mg)).

Cytotoxicity assays

The cytotoxicity of Col-HMNs (5 mg Col), HMNs, and 5 mg Col on against human keratinocytes (HaCaT) was tested using a CCK-8 kit. Before the study, the samples were soaked in 10 mL DMEM complete medium for 24 h, and HaCaT cells were seeded at a density of 1×10^6 cells per well on 96-well plates and cultured overnight. Then, the cells were incubated in the presence of the different soak solutions of samples for 24 h. The treated cells were incubated with 10% CCK-8 at 37 °C for 1 h. The absorbance was measured at 450 nm using a microplate reader. All measurements were performed in triplicate and repeated at least three times. Results are shown as a percent of cell viability in comparison with non-treated control cells.

Histopathological experiment and skin histiocyte apoptosis experiment

The abdomen skin of rats was shaved and epilated, and then treated with HMNs and Col-HMNs for 24 or 48 h, respectively. Abdomen skin tissues were respectively obtained after 24 and 48 h. The excised skin specimens were fixed in 10% neutral formalin for 18 h and embedded in paraffin wax. Skin sections (4 μm thick) were prepared and stained with hematoxylin and eosin (H&E) and TUNEL to evaluate histopathology and apoptosis. Inflammatory and apoptotic cells were observed under a microscope and laser scanning confocal microscope, respectively.

In vivo visualization of drug distribution in the rat skin with time

An *in vivo* imaging system (IVIS spectrum, USA) and calcein fluorescence were used to visualize the drug distribution in the skin of SD rats. Briefly, calcein-loaded HMNs and calcein-loaded CMC-DMNs were fabricated and manually inserted into the hairless skin of the part of the rat near the ankle joint and then covered with medical adhesive tape. After the MN patch was adhered for 2, 6, 12, 24, 36, and 48 h, respectively, the rat was anesthetized, the MN patch and tape were peeled off the skin, the administration site was cleaned, and then the fluorescence was directly observed using the IVIS spectrum. Furthermore, the average radiant efficiency was quantized using Living Image software.

MSU-induced acute gout arthritis model establishment

The acute gout arthritis model was induced with monosodium urate (MSU) in SD rats. A horizontal line was drawn at 5 mm above the ankle joint with an indelible marker to unify the measurement standard of the toe volume. Then, 0.2 mL MSU suspension (25 mg mL^{-1}) or 0.2 mL saline was injected into the rat ankle joint through a 21-gauge needle inserted just medial to the tendon of the tibialis anterior with its tip bev-

elled to 45°. The small volume changes of the rat toe volume were measured with a toe volume measuring device. The relation variation was calculated according to the change in the volume: the percent joint swelling ratio = $(V_t - V_0)/V_0 \times 100$, where V_t and V_0 represent the volume at different times and original volume, respectively.

Inhibitory effect of Col-HMNs against acute gout arthritis in rats

The rats were randomly divided into four groups: (1) the blank group, (2) the model group, (3) the Col-HMN group, and (4) the Col tablet (i.g. Col) group, with 12 rats in each group. Col-HMNs containing 1 mg Col were administered to the ankles of the rats in the Col-HMN group and fixed with medical tape. Similarly, rats in the Col tablet group were given 0.5 mg kg^{-1} aqueous solution of Col tablets (1 mg mL^{-1}). IL-1β, TNF-α, and IL-6 levels of the rat serum samples in the four groups were analyzed and determined using enzyme-linked immuno-sorbent assay (ELISA) kits following the manufacturer's instructions. The optical density was measured using a micro-plate reader. And then, the ankle joint tissue samples were fixed in 4% paraformaldehyde solution and decalcified with 10% EDTA embedded with paraffin. Sections were cut 6 μm thick, stained with HE, and pathologically examined under a light microscope. Moreover, the presence of plasma extravasa-tion in the synovial lavage samples was evaluated by measur-ing the total protein content, which was measured using the Bradford protein assay kit. Moreover, the presence of neutro-phils in the ankle joint tissue samples was evaluated through the measurement of MPO activity, which was measured using the myeloperoxidase assay kit.

Statistical analysis

SPSS (26 version) software was used to analyze all the experi-mental data. Results are presented as the mean ± standard error of the mean. Numerical variables between the two groups were tested using an unpaired *t*-test. Multiple compari-sons were performed using the one-way analysis of variance in combination with the Bonferroni *post hoc* test. Differences were considered significant at *$P < 0.05$, **$P < 0.01$ and ***$P < 0.001$.

Results and discussion

Design of tough and ultra-swellable microneedles for acute gout arthritis treatment

Tough and ultra-swellable microneedles were fabricated using an *in situ* photopolymerization method in a mold as shown in Fig. 1. Conventional synthetic hydrogels with a structural defect of multi-dispersed crosslinking points resulted in the prepared hydrogel with poor mechanical performance, which significantly reduced their potential and range of application. In this work, the commercial organic molecule (*N*,*N*′-bis (acrylyl)cysteamine, BACA) was used as the crosslinker contain-ing an ultraviolet light-responsive disulfide bond. When exposed to UV light, the disulfide bond can initiate bond clea-vage and chain exchange reactions, which could be helpful for modifying and improving the polymer network for well-distrib-uted architectures.[26,27] Moreover, polyacrylamide (PAM) chains with abundant donors and acceptors for forming hydrogen bonding and highly hydrophilic properties make the hydrogel microneedles mechanically tough with ultra-swelling pro-perties.[28] HMNs loaded with the hydrophilic drug colchicine could be easily obtained through the swelling process (Fig. 1a). As the HMNs were affixed to the joint skin of MSU-induced acute gout arthritis rats, the skin interstitial fluid would be effectively filled in the HMNs, triggering rapid diffusion of the preloaded Col into the skin tissue, which would reduce the levels of inflammatory cytokines IL-1β, IL-6, and TNF-α (Fig. 1b).

Fabrication and characterization of HMNs

In a typical experiment, the microneedle investigated in this work was prepared through a micromolding approach.[29,30] Briefly, desired amounts of AM, BACA, and Irgacure 2959 solu-tion were loaded into a PDMS mold with a 20 × 20 array. The resulting HMNs with a 20 × 20 array could be easily formed under UV irradiation in 30 min (Fig. 2a), and each microneedle possessed a conical shape with a height diameter of 500 μm and a base diameter of 300 μm. The structure of HMNs was further confirmed by optical and fluorescence microscopy (Fig. 2b and c). The fluorescence microscopy image also demonstrated that the calcein molecules were uniformly dis-tributed inside the real needles, and the loading process had no influence on the structure of the HMNs. As shown in the SEM images, the HMNs exhibited a symmetrical layer-shaped structure (Fig. 2d and e) and a regular porous structure after lyophilization (Fig. 2f), which facilitated high loading efficiency and stable diffusion of drugs.[31]

Furthermore, the corresponding mapping elemental pro-files of the HMNs were used to analyze the uniform structure. As shown in Fig. S1 (ESI†), the sulphur element was dispersed uniformly throughout the image, indicating that the cross-linking points are well distributed in the HMNs. Moreover, the critical role of the disulfide bond in the mechanical properties of microneedles was verified, as shown in Fig. 3a, and the HMNs exhibited extraordinary mechanical performances. The fracture force of HMNs measured using the texture analyzer at a displacement of 0.42 mm was 11.53 N per needle, which was larger than that of HMNs using *N*,*N*-methylene bisacrylamide (MBA) molecules (8.11 N per needle) as the crosslinker, further confirming the significant role of disulfide bonds. In addition, quantitative investigations of the mechanical and swelling per-formances of the HMNs could be performed by changing the mass ratio of the acrylamide monomer (AM), the crosslinking agent (BACA), and the photoinitiator (Irgacure 2959) in pre-gel solution (Table S1, ESI†). As shown in Fig. S2 (ESI†), the frac-ture force of the HMNs was 1.0–13.0 N per needle as the swell-ing ratio was 1000–3000%. Thus, the optimal values of AM, BACA, and Irgacure 2959 of the prepared HMNs were 16.67 wt%, 3.33 wt‰, and 8.33 wt‰ (H8), respectively.
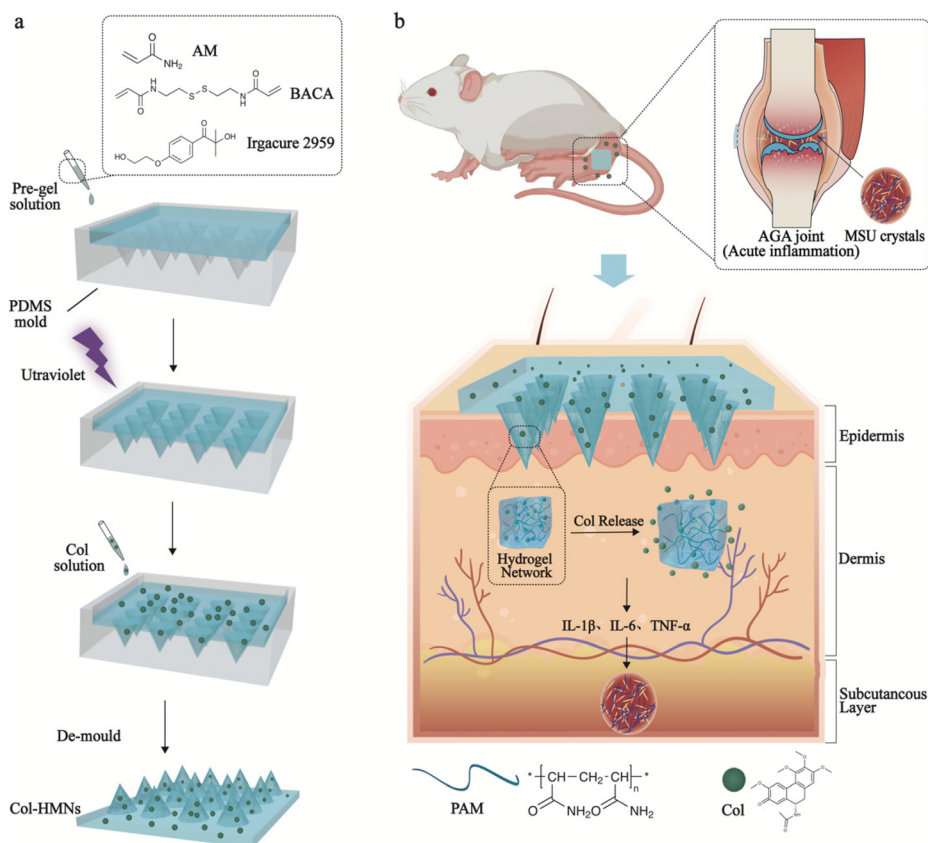
Fig. 1 Schematic of the fabrication process of a tough and ultra-swellable microneedle delivery system for acute gout arthritis treatment. (a) Schematic of the fabrication of a tough and ultra-swellable microneedle from a mold using an *in situ* photopolymerization method. (b) Colchicine (Col) was triggered to release by the diffusing process as the microneedles were used on the MSU-induced acute gout rats, resulting in the decreased levels of inflammatory cytokines IL-1β, IL-6, and TNF-α in MSU-induced acute gout rats.
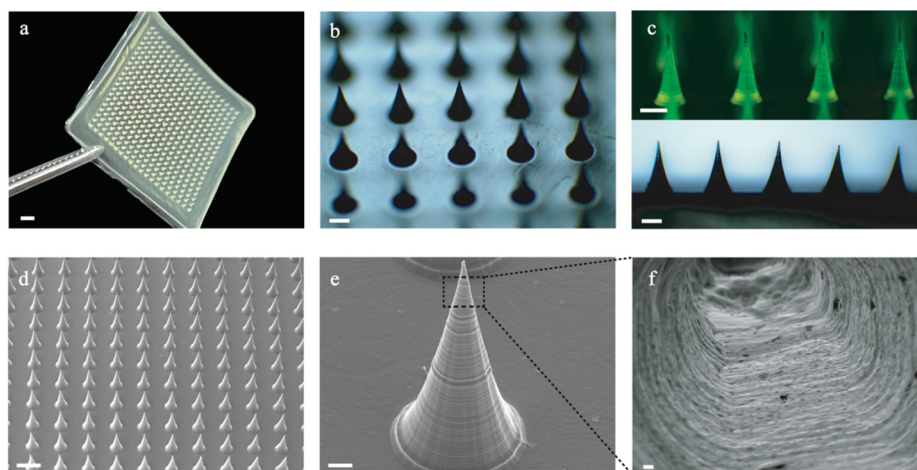
Fig. 2 Apparent characterization of HMNs. (a) Optical image of HMNs; scale bar: 2 mm. (b) Optical microscopy images of HMNs, 4×; scale bar: 200 μm. (c) Fluorescence microscopy images of calcein-loaded HMNs (up, 5×) and optical microscopy images of HMNs (down, 4×); scale bar: 200 μm. (d and e) SEM images of HMNs. Scale bar in (d), 500 μm; scale bar in (e), 50 μm. (f) SEM image of the lyophilized HMNs showing the porous structure; scale bar: 2 μm.
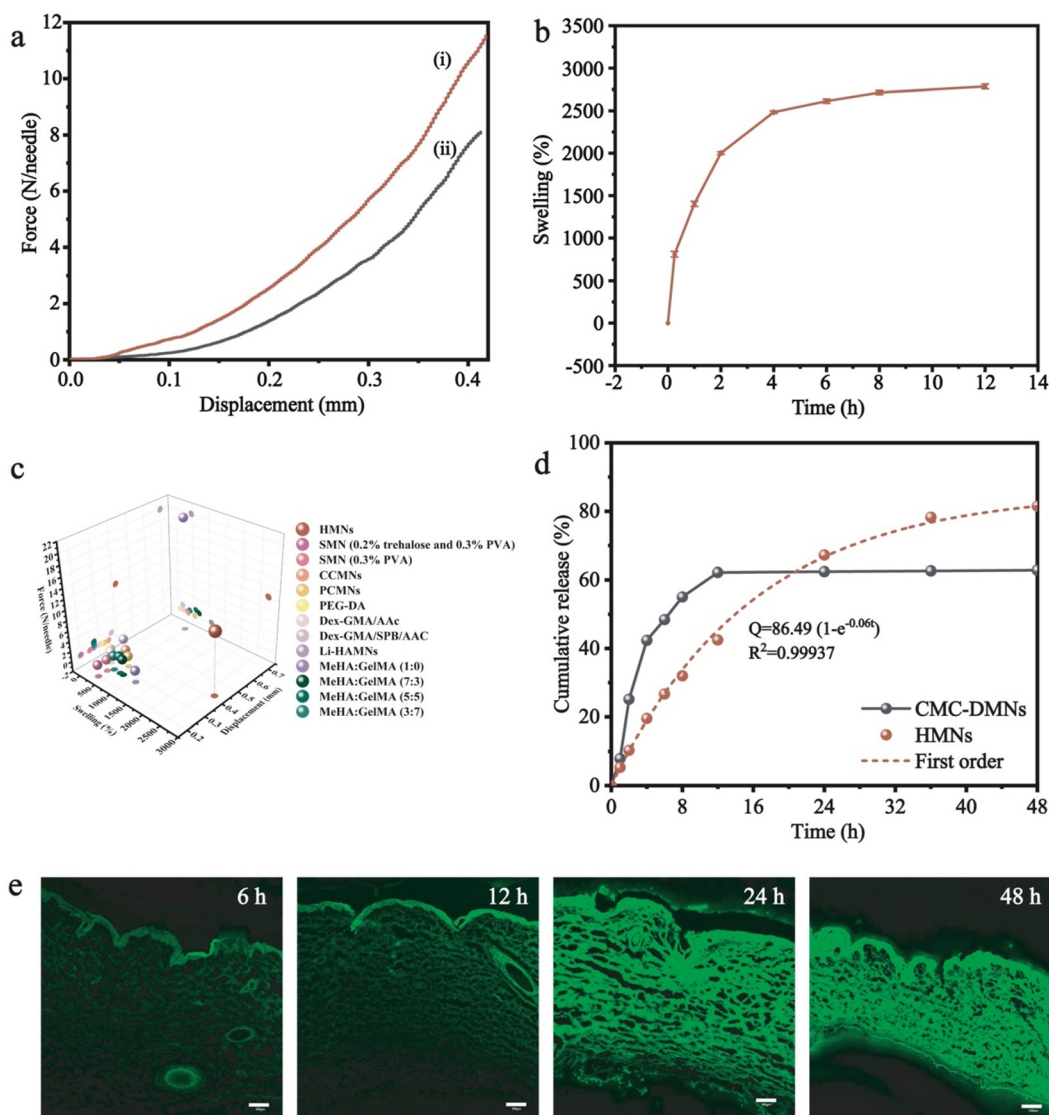
Fig. 3 *In vitro* performance characterization of HMNs and Col-HMNs. (a) Mechanical behavior of HMNs made of different crosslinkers: (i) BACA. (ii) MBA. (b) The swelling performance of HMNs (n = 3). (c) Comparison of the mechanical properties and swelling properties of HMNs in this study with hydrogel microneedles in the reported literature. (d) *In vitro* release kinetics of CMC-DMNs, Col from Col-HMNs (spots) and first-order kinetic fitting curve (dotted line, n = 3). (e) Fluorescence micrographs of the rat skin treated with calcein-loaded HMNs at different time intervals using a confocal laser scanning microscope. Scale bar: 100 μm.

Under the above conditions, the HMNs delivered a fracture force of 11.53 N per needle, and a swelling ratio of 2708% in 12 h (Fig. 3b). With excellent mechanical behavior, the HMNs could effectively penetrate the skin of the rats and pigs (Fig. S3, ESI†). It is worth noting that the performance of the HMNs was better than those of various previously reported HMNs in terms of mechanical strength and swelling ratio (Fig. 3c).[32–36] The excellent capabilities of the designed HMNs would provide a possibility for use in the thick cuticle skin using patches. However, the lack of flexibility of the HMNs limited the large area usage on the skin. To further reflect the strong superiority of the designed HMNs, a dissolving conventional microneedle (CMC-DMNs) prepared by CMC was fabricated. Both HMNs and CMC-DMNs could load 1 mg Col which met the dosage

requirement for clinical application and their average loading efficiency was higher than 95% (Fig. S4, ESI†). More than 80% of Col was released from Col-HMNs within 48 h and followed the first-order kinetics equation; nevertheless, the CMC-DMNs have a faster release rate and a lower cumulative release degree (Fig. 3d). This adjustable drug release behavior of the HMNs could avoid the toxic reaction caused by the burst release of Col. Additionally, fluorescence images were recorded to better observe the release of drugs from the HMNs. As shown in Fig. 3e, calcein was distributed uniformly on the skin even after 48 h when the calcein loaded HMNs were applied on the pig skin. The microscopy image of Col-HMNs showed that the addition of the Col did not influence the shape of the HMNs (Fig. S5, ESI†). For the FTIR spectrum of Col-HMNs, the peaks

assigned to N–H (3186, 1423 cm^{-1}), C–H (2928 and 1313 cm^{-1}) and C=O (1648 cm^{-1}) were just the same as that of HMN, indicating negligible influence of Col introduction (Fig. S6, ESI†). All the above results verified that the prepared HMNs could effectively penetrate the skin tissue and deliver the drugs to the dermis.

Biocompatibility *in vivo* and *in vitro*

A favorable biocompatibility and non-cytotoxicity are essential qualities of well-designed biomaterials. Here, the viability of HaCaT cells was employed to assess the cytocompatibility of HMNs.[37,38] Compared to the control group, there was a noticeable growth trend of HaCaT cell proliferation in the HMN group, and the Col-HMN group displayed more than 95% cell viability, higher than the blank Col group, indicating the favorable biocompatibility of the prepared HMNs and Col-HMNs (Fig. 4a). In addition, the cell morphology observation results showed that the cells grew well (Fig. S7, ESI†). Furthermore, to investigate the safety of HMNs deeply, the H&E staining and TUNEL staining of rat abdominal skin sections treated with HMNs and Col-HMNs for 24 and 48 h were performed. The section of the HMN treated skin showed almost similar cellular integrity as compared to the control skin. The section of the Col-HMN treated skin showed no inflammatory effects but cell proliferation was inhibited to a certain extent due to the binding effect of colchicine and microtubules.[39] Meanwhile, the TUNEL staining results in each group showed that the microneedle did not cause apoptosis before and after drug loading, indicating the excellent biocompatibility of HMNs and Col-HMNs (Fig. 4b).

In vivo visualization of drug distribution in the rat skin with time

To further investigate whether the drug loaded in the HMNs can sustainably penetrate the skin, the IVIS spectrum and calcein fluorescence were used to visualize the drug distribution in SD rats. After treatment with the calcein-loaded HMNs for 2, 6, 12, 24, 36 and 48 h, the average radiant efficiency of calcein released from HMNs increased gradually with time and remained high until 48 h. However, the average radiant efficiency was of calcein released from CMC-DMNs

which reached the peak at 12 h, and, decreased gradually with time, and became weaker at 48 h (Fig. 5a and b). The results indicated that calcein loaded into the CMC-DMNs could penetrate the skin faster and the HMNs sustainably delivered the drug into the skin as a drug reservoir and prolonged the residence time of the drug in the skin.

Inhibitory effect of Col-HMNs against MSU-induced acute gout in rats

To demonstrate the anti-inflammatory effect of the Col-HMNs *in vivo*, rats injected with monosodium urate (MSU) to induce acute gout arthritis were used as models, while saline was injected as the control.[40,41] After 24 h, the MSU-treated rats showed obvious ankle swelling compared with the saline-treated control (Fig. 6a). The ankle of the MSU group rats showed extensive swelling after MSU injection (Fig. 6b), which was similarly recapitulated as the swelling and spontaneous resolution of human acute gout attack.[42,43]

The therapeutic effect of Col-HMNs was evaluated from the joint swelling volume, inflammatory factor levels, plasma extravasation, and MPO activity. Specifically, at the end of the treatment, the volume of joint swelling in the model group increased by about 80%. In contrast, after Col-HMNs or i.g. Col treatment, the swelling volume of the joint increased to about 50% and gradually decreased to about 37% of the thickness of the model group (Fig. 6c and S8, ESI†). Previous studies have shown that the production and release of IL-1β are the first and most important events in gout inflammation, TNF-α can enhance the activity of neutrophils, and the proinflammatory cytokine IL-6 is the key to initiating innate immune response.[44,45] Synovial and ankle joint contact with sodium urate crystals leads to cell necrosis, macrophage release, neutrophil death, and inflammation.[46] Compared with the model group, the levels of IL-1β, IL-6, and TNF-α inflammatory cytokines were found to decrease after Col-HMN treatment, while similar results were obtained with the i.g. Col group (Fig. 6d–f). The cell necrosis and macrophages to the joint were pathological markers of AGA. Thus, HE staining from the rat ankle joint was further conducted.[47] As shown in Fig. 7, there was apparent inflammatory infiltration and focal necrosis in the model group, while the inflammation was sig-
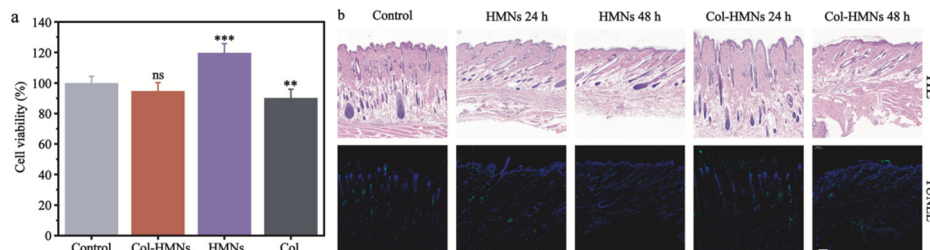

Fig. 4 Compatibility of HMNs *in vivo* and *in vitro*. (a) Viability of HaCaT cells after incubation with HMNs, Col-HMNs, and Col solution for 24 h (*n* = 3). The asterisks denote significance levels: *$P < 0.05$, ***$P < 0.01$, ***$P < 0.001$ *vs.* control. (b) H&E staining and TUNEL staining of rat abdominal skin (the apoptosis cell was green, and the nuclei were blue) with HMNs and Col-HMNs treated for 24 and 48 h. Scale bar: 200 μm.
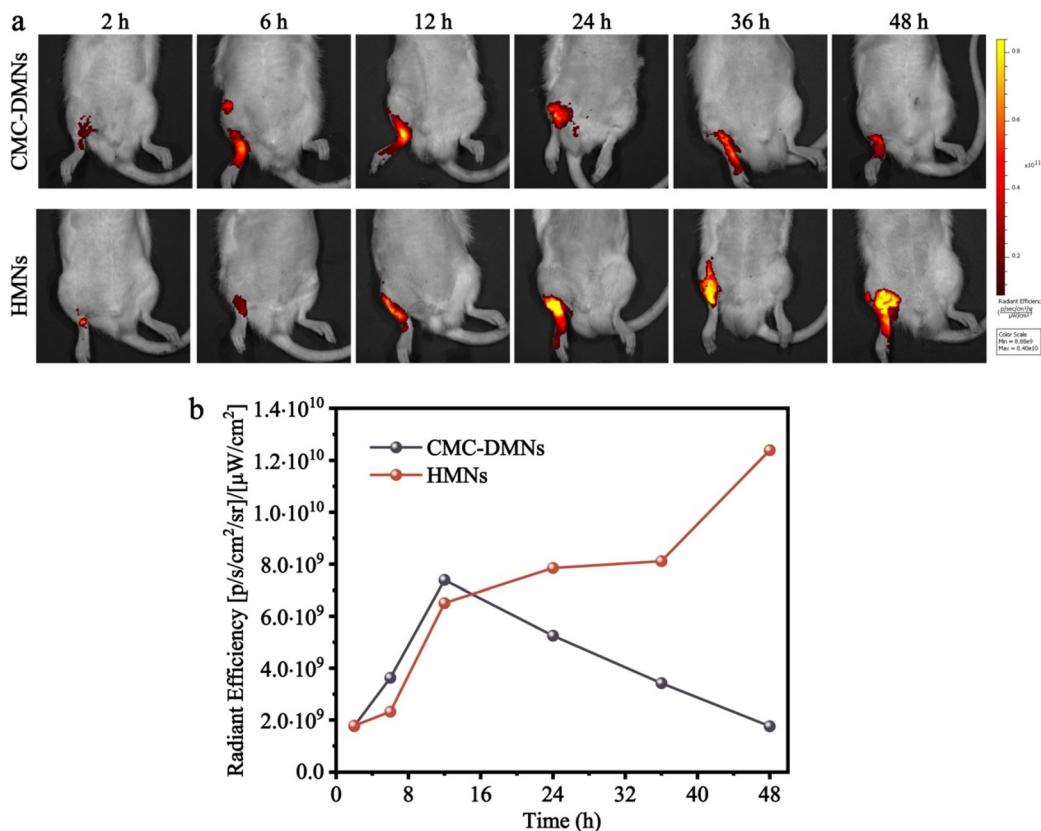
Fig. 5 *In vivo* imaging of rats after being treated with CMC-DMNs and HMNs. (a) *In vivo* images of calcein delivery from CMC-DMNs and HMNs into the ankle joint of rats for 48 h. (b) The average radiant efficiency with time.
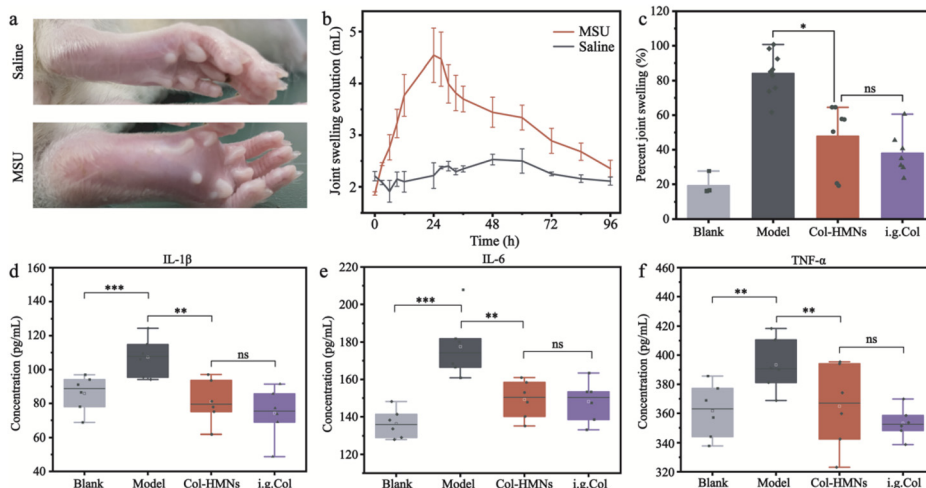

Fig. 6 Effect of Col-HMNs on ankle swelling and the levels of inflammatory cytokines in the rat. (a) Comparative images of edema after injection with monosodium urate (MSU) crystal suspension into the left ankle joint and saline injection into the right ankle joint. (b) Changes of the foot volume with time after injection with monosodium urate (MSU) crystal suspension and saline into the ankle joint of rats ($n = 6$). (c) The relation variation of the foot volume in rats treated with Col-HMNs and i.g. Col. (d–f) Concentration of the inflammatory factors IL-1 β (d), IL-6 (e), and TNF-α (f) in rat serum after treatment. Each point on the curve represents the mean (S.E.M.) of five to seven rats. The asterisks denote significance levels: *$P < 0.05$, **$P < 0.01$, ***$P < 0.001$. Two-way ANOVA was followed by Bonferroni's *post hoc* test.

Fig. 7 Histopathological changes in the ankle joint of the rats as assessed by H&E staining. H&E-stain sections from rat ankle joint at the end of treatment with Col-HMNs and i.g. Col. Black, red and yellow arrows represent macrophages, necrotic cells, and neutrophils, respectively; scale bar: 50 μm.

Fig. 8 Each group of rats responded to plasma extravasation and myeloperoxidase activity. The total protein content in the synovial lavage samples (a) and the MPO activity in the ankle joint tissue samples (b). Each point on the curve represents the mean (S.E.M.) of five to seven rats. The asterisks denote significance levels: $*P < 0.05$, $**P < 0.01$, $***P < 0.001$. Two-way ANOVA was followed by Bonferroni's *post hoc* test.

nificantly reduced in the Col-HMNs and i.g. Col groups. The inflammation also triggered a rise in plasma extravasation and MPO activity in 24 h.[48] Compared with the model group, the plasma protein concentration in the articular cavity of rats in the Col-HMN group and the i.g. Col group, respectively, decreased by 33.6% and 22.5% (Fig. 8a). The MPO activity of the ankle joint in the Col-HMNs group and the i.g. Col group respectively decreased by 53.5% and 56.5% (Fig. 8b). Hence, combined with the above results, we confirmed that the Col-HMs could contribute to the ability of AGA treatment.

Conclusions

Here, we have fabricated novel HMNs with mechanical and ultra-swelling properties and loaded with Col, providing a promising strategy for AGA treatment. The HMNs were prepared using a UV-responsive crosslinker with an ultraviolet light-responsive disulfide bond and an *in situ* photo-polymerization. *In vitro* and *in vivo* experiments indicated that the Col-HMNs with favorable biocompatibility could release Col when applied on the rat skin, and the sustained release of Col induced a decrease in the levels of inflammatory cytokines IL-1β, IL-6, and TNF-α in MSU-induced acute gout modeled rats. Our study used Col-loaded HMNs to offer a promising drug-delivering system for AGA treatment, while successful translation of the Col-HMN system will involve further phar-

macokinetics, high dosage efficacy, and dose-dependent toxicity studies conducted in small and large animal models and clinical research.

Author contributions

Suping Jiang: conceptualization, data curation, formal analysis, investigation, methodology, writing – review, and editing. Huanhuan Liu, Wensheng Zheng, Jiwen Zhang, and Can Peng: conceptualization, funding acquisition, writing – review, and editing. Jiming Ke, Wen Wang, Shan Huang, Jie Wang, Chengxi Luo, Xiaoxia Li, and Kaili Zhang: data curation and methodology. All authors have read and approved the final manuscript.

Conflicts of interest

The author(s) have no conflict of interest to declare.

Acknowledgements

References

1 N. Dalbeth, H. K. Choi, L. A. B. Joosten, P. P. Khanna, H. Matsuo, F. Perez-Ruiz and L. K. Stamp, *Nat. Rev. Dis. Primers*, 2019, **5**, 69.

2 N. Dalbeth, T. R. Merriman and L. K. Stamp, *Lancet*, 2016, **388**, 2039–2052.

3 E. Cipolletta, L. J. Tata, G. Nakafero, A. J. Avery, M. A. Mamas and A. Abhishek, *J. Am. Med. Assoc.*, 2022, **328**, 440–450.

4 W. Doehner, S. D. Anker, J. Butler, F. Zannad, G. Filippatos, J. P. Ferreira, A. Salsali, C. Kaempfer, M. Brueckmann, S. J. Pocock, J. L. Januzzi and M. Packer, *Eur. Heart J.*, 2022, **43**, 3435–3446.

5 B. J. McKenzie, M. D. Wechalekar, R. V. Johnston, N. Schlesinger and R. Buchbinder, *Cochrane Database Syst. Rev.*, 2021, **8**, CD006190.

6 A. Qaseem, R. P. Harris, M. A. Forciea, Clinical Guidelines Committee of the American College of Physicians, T. D. Denberg, M. J. Barry, C. Boyd, R. D. Chow, L. L. Humphrey, D. Kansagara, S. Vijan and T. J. Wilt, *Ann. Intern. Med.*, 2017, **166**, 58–68.

7 C. M. van Durme, M. D. Wechalekar, R. B. Landewe, J. Pardo Pardo, S. Cyril, D. van der Heijde and R. Buchbinder, *Cochrane Database Syst. Rev.*, 2021, **12**, CD010120.

8 S. Stewart, K. C. K. Yang, K. Atkins, N. Dalbeth and P. C. Robinson, *Arthritis Res. Ther.*, 2020, **22**, 28.

9 S. Bindu, S. Mazumder and U. Bandyopadhyay, *Biochem. Pharmacol.*, 2020, **180**, 114147.

10 S. H. Yu, A. M. Drucker, M. Lebwohl and J. I. Silverberg, *J. Am. Acad. Dermatol.*, 2018, **78**, 733–740.e711.

11 B. Yang, Y. Dong, Y. Shen, A. Hou, G. Quan, X. Pan and C. Wu, *Bioact. Mater.*, 2021, **6**, 2400–2411.

12 J. Chi, L. Sun, L. Cai, L. Fan, C. Shao, L. Shang and Y. Zhao, *Bioact. Mater.*, 2021, **6**, 3507–3514.

13 T. Waghule, G. Singhvi, S. K. Dubey, M. M. Pandey, G. Gupta, M. Singh and K. Dua, *Biomed. Pharmacother.*, 2019, **109**, 1249–1258.

14 S. Yao, Y. Wang, J. Chi, Y. Yu, Y. Zhao, Y. Luo and Y. Wang, *Adv. Sci.*, 2022, **9**, e2103449.

15 J. Yu, C. Kuwentrai, H. R. Gong, R. Li, B. Z. Zhang, X. Lin, X. Wang, J. D. Huang and C. Xu, *Acta Biomater.*, 2022, **148**, 133–141.

16 R. He, Y. Niu, Z. Li, A. Li, H. Yang, F. Xu and F. Li, *Adv. Healthcare Mater.*, 2020, **9**, e1901201.

17 N. Xu, M. Zhang, W. Xu, G. Ling, J. Yu and P. Zhang, *Analyst*, 2022, **147**, 1478–1491.

18 M. Yu, Z. Lu, Y. Shi, Y. Du, X. Chen and M. Kong, *Int. J. Biol. Macromol.*, 2021, **191**, 783–791.

19 T. Takigawa, H. Araki, K. Takahashi and T. Masuda, *J. Chem. Phys.*, 2000, **113**, 7640–7645.

20 K. Haraguchi and T. Takehisa, *Adv. Mater.*, 2002, **14**, 1120–1124.

21 M. Shibayama, *Macromol. Chem. Phys.*, 1998, **199**, 1–30.

22 W. Li, R. Feng, R. Wang, D. Li, W. Jiang, H. Liu, Z. Guo, M. J. Serpe and L. Hu, *J. Mater. Chem. B*, 2018, **6**, 4799–4807.

23 P. Ranjan Yadav, M. Iqbal Nasiri, L. K. Vora, E. Larraneta, R. F. Donnelly, S. K. Pattanayek and D. Bhusan Das, *Int. J. Pharm.*, 2022, **622**, 121835.

24 Z. Shu, Y. Cao, Y. Tao, X. Liang, F. Wang, Z. Li, Z. Li and S. Gui, *Drug Delivery*, 2020, **27**, 642–651.

25 Q. Yan, W. Wang, J. Weng, Z. Zhang, L. Yin, Q. Yang, F. Guo, X. Wang, F. Chen and G. Yang, *Drug Delivery*, 2020, **27**, 1147–1155.

26 H. Chen, C. Peng, L. Wang, X. Li, M. Yang, H. Liu, H. Qin and W. Chen, *Chem. Eng. J.*, 2021, **403**, 1385–8947.

27 C. N. Zhu, C. Y. Li, H. Wang, W. Hong, F. Huang, Q. Zheng and Z. L. Wu, *Adv. Mater.*, 2021, **33**, e2008057.

28 E. Laszlo, G. De Crescenzo, A. Nieto-Argüello, X. Banquy and D. Brambilla, *Adv. Funct. Mater.*, 2021, **31**, 2106061.

29 S. C. Balmert, C. D. Carey, G. D. Falo, S. K. Sethi, G. Erdos, E. Korkmaz and L. D. Falo, Jr., *J. Controlled Release*, 2020, **317**, 336–346.

30 R. Jamaledin, C. Di Natale, V. Onesto, Z. B. Taraghdari, E. N. Zare, P. Makvandi, R. Vecchione and P. A. Netti, *J. Clin. Med.*, 2020, **9**, 66.

31 Z. Yin, D. Kuang, S. Wang, Z. Zheng, V. K. Yadavalli and S. Lu, *Int. J. Biol. Macromol.*, 2018, **106**, 48–56.

32 Z. Zhou, M. Xing, S. Zhang, G. Yang and Y. Gao, *Int. J. Pharm.*, 2022, **618**, 121669.

33 X. Pan, Y. Li, W. Pang, Y. Xue, Z. Wang, C. Jiang, C. Shen, Q. Liu and L. Liu, *Int. J. Pharm.*, 2022, **617**, 121612.

34 J. Li, H. Lu, Y. Wang, S. Yang, Y. Zhang, W. Wei, Y. Qiao, W. Dai, R. Ge and H. Dong, *Anal. Chem.*, 2022, **94**, 968–974.

35 T. Zhu, X. Yu, X. Yi, X. Guo, L. Li, Y. Hao and W. Wang, *Pharmaceutics*, 2022, **14**, 686.

36 X. Q. Niu, D. P. Zhang, Q. Bian, X. F. Feng, H. Li, Y. F. Rao, Y. M. Shen, F. N. Geng, A. R. Yuan, X. Y. Ying and J. Q. Gao, *Int. J. Pharm.: X*, 2019, **1**, 100027.

37 Y. Liang, A. Simaiti, M. Xu, S. Lv, H. Jiang, X. He, Y. Fan, S. Zhu, B. Du, W. Yang, X. Li and P. Yu, *Nanomaterials*, 2022, **12**, 108247.

38 J. Yang, X. Liu, W. Wang, Y. Chen, J. Liu, Z. Zhang, C. Wu, X. Jiang, Y. Liang and J. Zhang, *Bioelectrochemistry*, 2022, **148**, 108247.

39 Z. Chen, H. Li, Y. Bian, Z. Wang, G. Chen, X. Zhang, Y. Miao, D. Wen, J. Wang, G. Wan, Y. Zeng, P. Abdou, J. Fang, S. Li, C. J. Sun and Z. Gu, *Nat. Nanotechnol.*, 2021, **16**, 933–941.

40 C. Wu, S. Chen, Y. Liu, B. Kong, W. Yan, T. Jiang, H. Tian, Z. Liu, Q. Shi, Y. Wang, Q. Liang, X. Xi and H. Xu, *Bioengineered*, 2022, **13**, 11782–11793.

41 M. Zhou, K. Ze, L. Hua, L. Liu, L. Kuai, M. Zhang, B. Li, Y. Wang and X. Li, *Mediators Inflammation*, 2020, **2020**, 8298615.

42 J. J. Cheng, X. D. Ma, G. X. Ai, Q. X. Yu, X. Y. Chen, F. Yan, Y. C. Li, J. H. Xie, Z. R. Su and Q. F. Xie, *Drug Des., Dev. Ther.*, 2022, **16**, 2119–2132.

43 Y. X. Shang, X. Dong, Z. M. Xie, X. P. Li, X. C. Wang, J. Y. Huang, S. F. Wei, Y. Liu and J. P. Liu, *Trials*, 2022, **23**, 387.

44 S. Bodofsky, T. R. Merriman, T. J. Thomas and N. Schlesinger, *Semin. Arthritis Rheum.*, 2020, **50**, 1089–1100.

45 N. Dalbeth, T. J. Lauterio and H. R. Wolfe, *Clin. Ther.*, 2014, **36**, 1465–1479.

46 J. Desai, S. Steiger and H. J. Anders, *Trends Mol. Med.*, 2017, **23**, 756–768.

47 Z. Lan, L. Chen, J. Feng, Z. Xie, Z. Liu, F. Wang, P. Liu, X. Yue, L. Du, Y. Zhao, P. Yang, J. Luo, Z. Zhu, X. Hu, L. Cao, P. Lu, R. Sah, K. Lavine, B. Kim and H. Hu, *Ann. Rheum. Dis.*, 2021, **80**, 1604–1614.

48 C. Hoffmeister, M. A. Silva, M. F. Rossato, G. Trevisan, S. M. Oliveira, G. P. Guerra, C. R. Silva and J. Ferreira, *Rheumatology*, 2014, **53**, 240–249.